DOI: 10.1002/adma.200801205

Tunable Magnetism in Carbon-Ion-Implanted Highly Oriented Pyrolytic Graphite**

By *Huihao Xia,* Weifeng Li, You Song, Xinmei Yang, Xiangdong Liu, Mingwen Zhao,* Yueyuan Xia, Chen Song, Tian-Wei Wang, Dezhang Zhu, Jinlong Gong,* and *Zhiyuan Zhu*

Reports of magnetism at room temperature (RT) in pure carbon materials[1,2] have stimulated studies to determine the origin of magnetism in these materials, and to explore prospective applications. The experimental evidence for ferromagnetism in proton-irradiated highly oriented pyrolytic graphite (HOPG)[3,4] has provided further support of the existence of carbon magnetism. However, the origin of magnetic order in pure carbon is only poorly understood, and for many years some scientists doubted the possibility of RT ferromagnetism in these materials, which have only s and p electrons, as it was usually believed that it is only possible in materials containing metallic 3d or 4f electrons. The situation changed last year when a collaborative group of US and German scientists provided the first direct experimental evidence of π-electron ferromagnetism in metal-free carbon films by using X-ray magnetic circular dichroism (XMCD).[5] This finding may provide a new impetus for studies of applications of magnetic carbon-based materials in diverse fields.

Magnetism of carbon materials is of particular interest as the lightweight, cheap magnets could open up new ways to design adaptable and flexible information storage systems. The potential application of carbon-based magnets in spin electronics is promising, since carbon may provide an easy way to integrate spin and molecular electronics. The long diffusion lengths and coherent times arising from the weak spin–orbit and hyperfine interactions in carbon can provide ideal conditions for coherent spin manipulation. Very recently, manipulation of spin states of a carbon nanotube quantum dot connected to two ferromagnetic electrodes was realized by tuning the gate voltage.[6] Theoretical study indicated that the magnetic properties of nanometer-scale zigzag graphene ribbon can be controlled by an external electric field.[7] These are very encouraging findings in spintronics, where carbon magnetism could play an important role. Biocompatible carbon magnets could be used in implantable bioelectronic devices and in medicine, for instance as biosensors.[8–10] Furthermore, carbon magnetism will attract interest in biophysical and chemical sciences because the spin-dependent part of the electronic wavefunction can affect the chemical bonding path, as has been found in selective growth of diamond using a magnetic field.[11] For all these potential applications, the following key problems must be solved adequately: The ferromagnetic state in the pure carbon materials must be stable at or above RT; reliable and easy methods must be established to produce magnetization large enough for practical application of the magnetic carbon materials; proper methods must be developed to provide the possibility of fine-tuning of the magnetization in these materials; and thorough theoretical methods must be developed to give a better understanding of the origin of the magnetism in pure carbon materials and to provide guidelines for design of more subtle magnetic carbon devices.

Applying our efforts to these problems, we have worked out an experimental method to induce macroscopic magnetization (as large as 9.3 emu g^{-1}) at RT in HOPG samples by using $^{12}C^{+}$ ion implantation. We find that the ferromagnetic critical temperature, T_c, of the sample is about 460 K. The implantation-induced magnetic moments in the sample can be tuned simply by changing the implantation dose. Using spin-polarized density functional theory (DFT), we have obtained the electronic structures of the graphite lattice containing magnetic defects that mimic the defects produced by $^{12}C^{+}$ ion bombardment. They clearly show long-range magnetic coupling in the defective graphite lattice and provide theoretical support for proposition that the ferromagnetic order in the defective lattice originates from the π-electrons from the magnetic defects. This is in agreement with recent experimental findings.[5]

[*] Dr. H. H. Xia, Prof. D. Z. Zhu, J. L. Gong, Z. Y. Zhu
Key Laboratory of Nuclear Analysis Technique
Shanghai Institute of Applied Physics
Chinese Academy of Sciences
Shanghai 210800 (P. R. China)
E-mail: hxia@sinap.ac.cn

Prof. M. W. Zhao, W. F. Li, X. M. Yang, X. D. Liu, Y. Y. Xia, Dr. C. Song
Department of Physics
School of Physics
Shandong University
Jinan, Shandong 250100 (P. R. China)
E-mail: zmw@sdu.edu.cn

Prof. Y. Song, T.-W. Wang
State Key Laboratory of Coordination Chemistry
School of Chemistry and Chemical Engineering
Nanjing University
Nanjing 210093 (P. R. China)

[**] The work reported here was supported by the Knowledge Innovation Program of the Chinese Academy of Sciences under grant no. KJCX3-SYW-N10 and by the National Natural Science Foundation of China under grant nos. 10705047, 10675075, and 50402017. We thank the National Basic Research Program of China for funding support under grant no. 2005CB623602. Supporting Information is available online from Wiley InterScience or from the authors.

ADVANCED MATERIALS

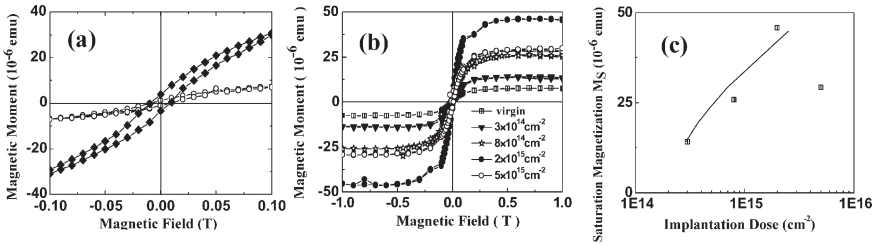

Figure 1. a,b) Magnetic moments measured at 300 K for HOPG samples. a) Hysteresis loops measured for the HOPG sample before ion implantation (empty circles) and after ^{12}C ion implantation (dose 2×10^{15} cm^{-2}, solid diamonds) for an applied magnetic field between -0.1 T and $+0.1$ T. b) Measured magnetic moments as a function of the applied magnetic field, cycled between -1.0 T and $+1.0$ T, for the virgin HOPG sample and after $^{12}C^{+}$ implantation in the sample, different doses. c) The measured saturation magnetic moment as a function of the implantation dose.

In our experiments, ion implantations and magnetic measurements were performed on HOPG samples, four consecutive implantation stages for each sample. Before implantation and after each implantation stage, the magnetic moments of the sample assembly were measured at 300 K, and after the fourth implantation stage measurements were performed at different temperatures (5 K to 350 K) to examine the temperature dependence of the magnetic moments. Details of the experimental setup and doses 1–4 can be found in the Experimental section.

Figure 1a and b show the measured magnetic moments of the sample at 300 K, after subtraction of the diamagnetic background. Figure 1a depicts the magnetic hysteresis loops for the virgin sample (open circles) and the sample implanted with a dose of 2×10^{15} cm^{-2} (solid diamonds) in a low field from -0.1 T to 0.1 T. The loop of the implanted sample clearly shows ferromagnetic behavior. Figure 1b shows the magnetic moments measured after each implantation stage for an applied magnetic field cycled between -1.0 T and 1.0 T. Figure 1c depicts the measured saturation magnetic moment as a function of the implantation dose. For the doses ranging from 3×10^{14} cm^{-2} to 2×10^{15} cm^{-2}, the saturation magnetic moment increases with increasing implantation dose, N_d, in accordance with a power law, $M_s \approx 7.2 \times 10^{-6}$ $(N_d/10^{14}\,\text{cm}^{-2})^{0.62}$ emu (the solid curve in Fig. 1c). However, when the dose increases to 5×10^{15} cm^{-2}, the saturation magnetic moment decreases substantially. This indicates that further increase of the implantation dose may create too high a defect density, leading to reduction of the magnetic moments induced by the defects,[12] and the lattice disorder, perhaps even amorphous zones in the lattice, may destroy the band structure and carrier density that are necessary for magnetic coupling.[4,13] This suggests that there is a dose window that can be used to tune the magnetization in HOPG.

According to the range and stopping theory and SRIM03 simulations[14] for 70 keV $^{12}C^{+}$ implantation in a carbon target, the implanted C atoms and the produced defects are restricted to a near-surface layer of thickness of ca. 243 nm. Thus the magnetic moments induced by the implantation are restricted to this layer. Taking the total penetration depth of the C ions into account, we obtain the maximum magnetization M induced by 2×10^{15} cm^{-2} $^{12}C^{+}$ implantation to be about 9.3 emu g^{-1}.

Figure 2a shows the magnetic moments, measured at temperatures ranging from 5 K to 350 K, as a function of the applied magnetic field for the sample implanted with dose 5×10^{15} cm^{-2}. Figure 2b gives the result measured in the low-field range. Figure 2c shows the normalized remanent magnetic moment $M_r/M_r(0)$ as a function of temperature for the sample. The measured data (solid squares with error bars) can be fitted with a straight line (dashed line). It indicates that, for temperatures lower than 350 K, the temperature dependence of the magnetization can be described by spin-wave theory based on a uniaxially anisotropic 2D Heisenberg model,[13,15] which predicts a linear dependence with temperature T at low temperature. The ferromagnetic critical temperature T_c is obviously higher than 350 K. The solid curve in Figure 2c represents the normalized

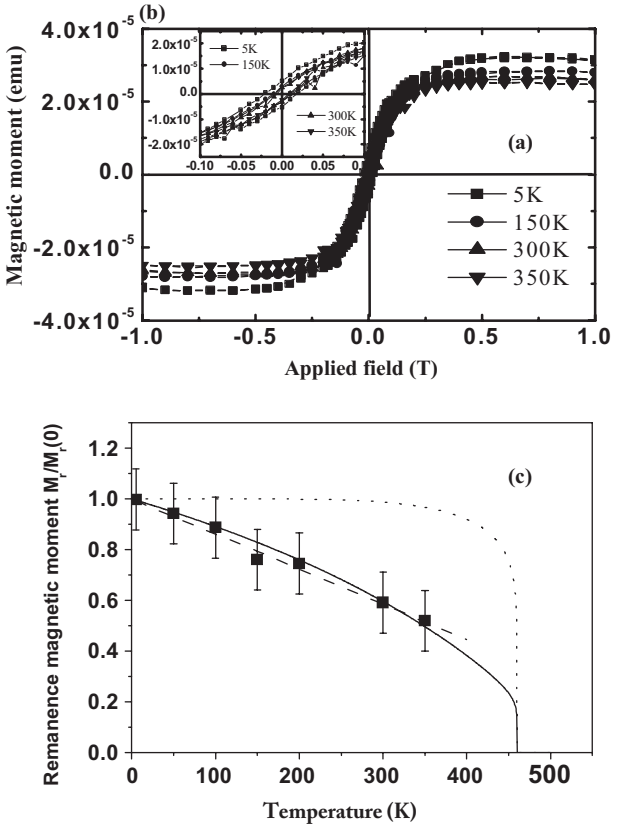

Figure 2. a) The magnetic moments measured at temperatures ranging from 5 K to 350 K, as a function of the applied magnetic field for the sample implanted with dose 5×10^{15} cm^{-2}. b) Low-field data. c) The normalized remanent magnetic moment as a function of temperature T measured for the sample, comparing the experimental data with the spin-wave theory in conjunction with the Ising model.

spontaneous magnetic moment as a function of T, which is obtained from perturbation theory up to third order for spin-wave magnetization[13,15] in conjunction with an Ising model[16] considering the spin-flip effect near the critical temperature (see Supporting Information). The dotted curve in Figure 2c is from the Ising model. It is clear that the theoretical model (solid line) fits the experimental data very well using the fitting parameters $T_c^{SW} = 1\,010$ K (spin-wave critical temperature), $\Delta = 0.01$ (the anisotropy constant), and $T_c = 460$ K (Supporting Information). Thus a critical temperature $T_c \approx 460$ K, is deduced for the $^{12}C^+$-ion-implanted HOPG sample.

Paramagnetism of proton-irradiated HOPG[17] and pure carbon sp^2-clustered graphitic structures[18] was reported recently. We also studied the temperature dependence of the magnetic moments at applied magnetic field $B = 1$ T for the HOPG sample implanted with a dose of 5×10^{15} cm^{-2}. Two contributions, a Curie-law-like component and a ferromagnetic contribution, are obtained. The total magnetic moment as a function of temperature can be fitted as

$$M(T) = \frac{1.5 \times 10^{-5}\ \text{emu K}}{T} + 2.83 \times 10^{-5}\ \text{emu} \qquad (1)$$

for temperatures below 300 K. A paramagnetic contribution at low temperature, which is larger than that of the virgin sample, indicates that some defects induced by the irradiation are responsible for the observed paramagnetic property at low temperature. From the Curie constant

$$C = \frac{NJ(J+1)g^2\mu_B^2}{3k_B} \qquad (2)$$

we estimate the density of the paramagnetic centers $N \approx 2.89 \times 10^{19}/V_0$ cm^{-3}, for $gJ \approx 1$, where V_0 is the effective volume of the sample.

To search for the possible origin of the magnetic ordering, we investigated the magnetic properties and the electronic structures of the defective HOPG using spin-polarized DFT, since previous theoretical studies[12,19–22] had indicated that defects in graphite or graphene layers can induce magnetic moments. The plane wave basis Vienna ab initio simulation package (VASP)[23,24] was used in the calculations (see Supporting Information).

Among various defect structures in graphite,[25] vacancies (A site and B site) — either a bare vacancy or a hydrogen-attached vacancy — can induce magnetic moments.[19–22] Besides vacancies, our calculation indicates that the rhombohedral defect, referred to as the r-defect hereafter (see Fig. 2c of the publication by Li et al.[25] for the structure), also induces magnetic moments in graphite. The electron spin density contours, the energy bands, the electron density of states (DOS), and the projected density of states (PDOS) on some orbitals of individual atoms near the defects for r-defects and vacancies are shown in Figures 3a and 3b, respectively. The distance between the two nearest defects is used to mimic the defect density in the lattice by using periodic boundary conditions for the supercell. Figure 3a (left column) shows the spin density contours around two r-defects with a separation of 7.4 Å, on the basal plane of the graphite. The r-defect structure is shown at the top of the left column of the figure, with the relevant atoms labeled 1, 2, and 3. The spin density distribution shown in this figure indicates that the spin density around each carbon atom is coupled in an antiparallel fashion to that on its nearest neighbor, leading to a long-range spin polarization

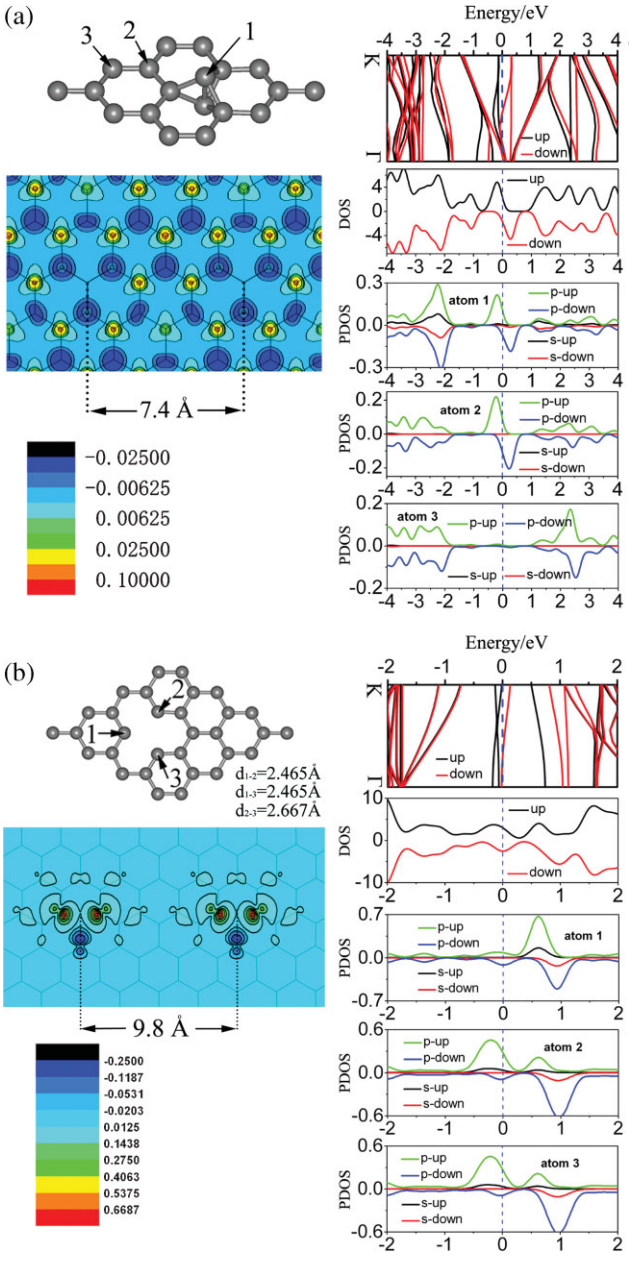

Figure 3. Spin density contours, energy bands, DOS and PDOS for a) a defective graphite lattice with r-defect separation of 7.4 Å, and b) a defective graphite lattice with vacancy separation of 9.8 Å.

ADVANCED MATERIALS

(order) on the basal plane of the graphite lattice. This coupling feature is consistent with Lieb's theorem[26] based on the Hubbard Hamiltonian on a bipartite lattice. The right column of Figure 3a shows (from top to bottom) the energy bands, the DOS, and the PDOS (DOS projected on the orbitals to specify the contributions from individual orbitals of the atoms labeled 1, 2, and 3, shown at the top of the left column). It is obvious that there is a narrow energy band around the Fermi level induced by the r-defects, referred to as the ''impurity'' band.[27] The itinerant electrons can occupy the partially filled ''impurity'' band, in which the carriers are spin polarized due to electron—electron interactions.[27] The DOS and PDOS in this figure confirm that the atoms around the r-defects give rise to this ''impurity'' band. The total DOS shows that the spin-up (majority spin, in black) and the spin-down (minority spin, in red) states are asymmetric at the Fermi energy, that is, the carriers in the band are spin polarized. From the PDOS it is evident that the p orbitals of atom 1 and atom 2 around the r-defects give rise to the splitting of the spin states (spin-up (green), spin-down (blue)) at the Fermi energy. The electrons occupying these states are spin-polarized π-electrons, which are responsible for the RT ferromagnetic order in the graphite. This completely agrees with recent experimental findings.[5] The splitting, shifting, and broadening of the resonance peak at the Fermi energy to form two peaks is due to interactions of the electrons and electron hopping between different sublattices (the nearest neighbor) and between the same sublattice (the next-nearest neighbor) in the graphite, as predicted in previous work.[27,28]

Figure 3b (left column) shows the spin density contour around two vacancies separated by a distance of 9.8 Å on the basal plane of the graphite. The vacancy structure and the three labeled carbon atoms around the vacancy are shown at the top of the column. The spin density distribution around the vacancies is different from that of the r-defects. The magnetic moments induced by the vacancies are more localized. However, we find that for this vacancy density (vacancy separation of 9.8 Å) the lattice deformation range around the vacancy is greater than the vacancy separation, and electrons are transferred from the B-sublattice to the A-sublattice (Supporting Information). This indicates that, through the deformation field surrounding the vacancies and the interaction between the nearest neighbors, the local moments are also coupled. This can be understood from analysis of the energy bands, the DOS, and the PDOS shown in the right column of Figure 3b. The vacancies also produce narrow ''impurity'' bands at the Fermi level, in which the electrons are spin polarized with high resonance DOS. The PDOS shown in this figure give clear evidence that the p orbitals of atom 2 and atom 3 around the vacancy give rise to spin-polarized states in the ''impurity'' bands. Similar to the case of r-defects, the electrons occupying these states are spin-polarized π-electrons. Therefore, for the defect density in the graphite lattice considered here to mimic the carbon-implantation-induced defects, our theoretical study predicts that the RT ferromagnetism observed in carbon-ion-implanted graphite is likely due to itinerant π-electrons that occupy the defect-induced impurity'' bands around the Fermi energy. For lower defect densities, the situation is different (Supporting Information). For bare vacancy defects in graphite, we find that the ferromagnetic states have no energy gap and the defective graphite is semimetallic. This is different from the case reported by Pisani et al.,[22] where the two dangling bonds of the vacancy in graphene were saturated by hydrogen atoms. In their case the defective graphene became semiconducting with an energy gap. We find that hydrogen saturation for dangling bonds of vacancies can also open a gap in the defective graphite. In this case the magnetic coupling, as proposed by Pisani et al.,[22] may be due to an instability in the π-electron system with respect to a long-range spin polarization characterized by alternation in the spin direction between adjacent carbon atoms.

In summary, we find that low-energy carbon-ion implantation can produce stable RT ferromagnetism in HOPG. The Curie temperature of the ferromagnetic phase is found to be as high as 460 K. The magnetization produced can be easily tuned by controlling the implantation dose with a tuning factor as large as three. The theoretical result indicates that the RT ferromagnetic order likely originates from itinerant π-electrons, in good agreement with recent experimental observations.[5]

Experimental

HOPG (ZYA grade) samples from NTMDT Inc., with a content of magnetic metallic impurities below 1 μg per gram of carbon, were used. The dimensions of the sample were 3 mm × 3 mm × 0.5 mm. The back of the sample was stuck on adhesive tape, which was used to mount the sample in the subsequent ion implantations and magnetic measurements. The implantation was performed at room temperature with a 70 keV $^{12}C^{+}$ beam. Four consecutive implantation stages were used for the same chosen sample, that is, the doses for stages 1 to 4 were 3×10^{14}, 8×10^{14}, 2×10^{15}, and 5×10^{15} cm^{-2}, respectively. In the magnetic moments measurement, the sample, together with the adhesive tape, was mounted in a plastic tube. Before the implantation and after each implantation stage, the magnetic moments of the sample assembly were measured at 300 K with a superconducting quantum interferometer device (SQUID) magnetometer from Quantum Design with a sensitivity of $\leq 10^{-7}$ emu. After stage 4 implantation (dose 5×10^{15} cm^{-2}), the SQUID measurements were performed at different temperatures, ranging from 5 K to 350 K, to examine the temperature dependence of the magnetic moments. Proton-induced X-ray emission (PIXE) spectra with a micro-beam were measured for the plastic tube and the adhesive tape; there were no detectable magnetic metal signals. PIXE spectra were measured for the virgin HOPG sample and the sample after each implantation stage to check the impurities. We found that the Fe impurity was less than 1 μg per gram of graphite, and the other magnetic metal impurities were below the detection limit of PIXE. For 1 μg of Fe impurities per gram of carbon in the sample, the maximum contribution of Fe to the magnetic moment would be less than 2.6×10^{-6} emu. In the SQUID measurement the applied magnetic field was perpendicular to the *c*-axis of the HOPG.

Received: May 1, 2008
Revised: June 6, 2008
Published online: October 15, 2008

[1] *Carbon-Based Magnetism*, (Eds: T, Makarova, F. Palacio), Elsevier, Amsterdam **2006**.
[2] P. Esquinazi, A. Setzer, R. Höhne, C. Semmelhack, Y. Kopelevich, D. Spemann, T. Butz, B. Kohlstrunk, M. Lösche, *Phys. Rev. B* **2002**, *66*, 024429.
[3] K.-H. Han, D. Spemann, P. Esquinazi, R. Höhne, V. Riede, T. Butz, *Adv. Mater.* **2003**, *15*, 1719.
[4] P. Esquinazi, D. Spemann, R. Höhne, A. Setzer, K.-H. Han, T. Butz, *Phys. Rev. Lett.* **2003**, *91*, 227201.
[5] H. Ohldag, T. Tyliszczak, R. Höhne, D. Spemann, P. Esquinazi, M. Ungureanu, T. Butz, *Phys. Rev. Lett.* **2007**, *98*, 187204.
[6] J. R. Hauptmann, J. Paaske, P. E. Lindelof, *Nat. Phys.* **2008**, *4*, 373.
[7] Y.-W. Son, M. L. Cohen, S. G. Louie, *Nature* **2006**, *444*, 347.
[8] M. Shim, N. W. S. Kam, R. J. Chen, Y. Li, H. Dai, *Nano Lett.* **2002**, *2*, 285.
[9] K. Besteman, J.-O. Lee, F. G. M. Wiertz, H. A. Heering, C. Dekker, *Nano Lett.* **2003**, *3*, 727.
[10] J. N. Wohlstadter, J. L. Wilbur, G. B. Sigal, H. A. Biebuyck, M. A. Billadeau, L. Dong, A. B. Fischer, S. R. Gudibande, S. H. Jameison, J. H. Kenten, J. Leginus, J. K. Leland, R. J. Massey, S. J. Wohlstadter, *Adv. Mater.* **2003**, *15*, 1184.
[11] R. B. Little, R. Goddard, *J. Appl. Phys.* **2004**, *95*, 2702.
[12] Y. Zhang, S. Talapatra, S. Kar, R. Vajtai, S. K. Nayak, P. M. Ajayan, *Phys. Rev. Lett.* **2007**, *99*, 107201.
[13] J. Barzola-Quiquia, P. Esquinazi, M. Rothermel, D. Spemann, T. Butz, N. García, *Phys. Rev. B* **2007**, *76*, 161403 (R).
[14] J. F. Ziegler, J. P. Biersack, U. Littmark, in *The Stopping and Range of Ions in Solids*, (Ed: J. F. Ziegler,), Pergamon, New York **1985**.
[15] P. A. Serena, N. García, A. Levanyuk, *Phys. Rev. B* **1993**, *47*, 5027.
[16] C. N. Yang, *Phys. Rev.* **1952**, *85*, 808.
[17] J. Barzola-Quiquia, P. Esquinazi, M. Rothermel, D. Spemann, A. Setzer, T. Butz, *Nucl. Instrum. Methods Phys. Res, Sect. B* **2007**, *256*, 412.
[18] J. M. Calderón-Moreno, A. Labarta, X. Batlle, D. Crespo, V. G. Pol, S. V. Pol, A. Gedanken, *Carbon* **2006**, *44*, 2864.
[19] P. O. Lehtinen, A. S. Foster, A. Ayuela, A. Krasheninnikov, K. Nordlund, R. M. Nieminen, *Phys. Rev. Lett.* **2003**, *91*, 017202.
[20] P. O. Lehtinen, A. S. Foster, Y. Ma, A. V. Krasheninnikov, R. M. Nieminen, *Phys. Rev. Lett.* **2004**, *93*, 187202.
[21] O. V. Yazyev, L. Helm, *Phys. Rev. B* **2007**, *75*, 125408.
[22] L. Pisani, B. Montanari, N. M. Harrison, *New J. Phys.* **2008**, *10*, 033002.
[23] G. Kresse, J. Furthmüller, *Comput. Mater. Sci.* **1996**, *6*, 15.
[24] G. Kresse, J. Furthmüller, *Phys. Rev. B* **1996**, *54*, 11169.
[25] L. Li, S. Reich, J. Robertson, *Phys. Rev. B* **2005**, *72*, 184109.
[26] E. H. Lieb, *Phys. Rev. Lett.* **1989**, *62*, 1201.
[27] D. M. Edwards, M. I. Katsnelson, *J. Phys: Condens. Matter* **2006**, *18*, 7209.
[28] V. M. Pereira, F. Guinea, J. M. B. Lopes dos Santos, N. M. R. Peres, A. H. Castro Neto, *Phys. Rev. Lett.* **2006**, *96*, 036801.